frontiers in Energy Research

ORIGINAL RESEARCH
published: 17 March 2022
doi: 10.3389/fenrg.2022.756900

Advancing Microbial Electrolysis Technology *via* Impedance Spectroscopy and Multi-Variate Analysis

Lucas R. Timmerman[1], *Sankar Raghavan*[2] *and Abhijeet P. Borole*[1,2]*

[1]Electro-Active Technologies Inc., Knoxville, TN, United States, [2]Chemical and Biomolecular Engineering, The University of Tennessee, Knoxville, TN, United States

In this study, EIS data collected from three electrode half-cell configurations was used to qualitatively identify and quantitatively determine the responses of ohmic, kinetic, and mass transfer impedances to buffer concentration, flow rate, and applied potential in an MEC consisting of a bioanode and an abiotic nickel-mesh cathode separated by a microporous membrane. EIS measurements were collected during startup and growth (including an abiotic run) at closed circuit and open circuit conditions to accurately match portions of the EIS spectra with the corresponding physical processes and to quantify kinetic changes as the biofilm matured. Once the MEC reached a target current density of 10 A/m^2, a multifactorial experimental design formulated as a Taguchi array was executed to assess the impact of flow rate, buffer concentration, and applied voltage on EIS and performance response variables. Multivariate analysis was conducted to ascertain the relative importance of the independent variables and identify any correlations between process conditions and system response. The liquid flow through the anode was found to be strongly correlated with the impedance parameters and the MEC performance, while applied voltage influenced them to a lesser degree. The results are important from an industrial application perspective and provide insights into parameters important for process optimization.

Keywords: microbial electrolysis, bioelectrochemical, renewable hydrogen, bio-electro-refinery, impedance spectroscopy

OPEN ACCESS

Edited by:
Dongwon Ki,
Seoul Institue of Technology, South Korea

Reviewed by:
Ioannis Andrea Ieropoulos,
University of Southampton, United Kingdom
G. Velvizhi,
Indian Institute of Chemical Technology (CSIR), India

****Correspondence:***
Abhijeet P. Borole
aborole@utk.edu

Specialty section:
This article was submitted to Bioenergy and Biofuels, a section of the journal Frontiers in Energy Research

Received: *11 August 2021*
Accepted: *28 February 2022*
Published: *17 March 2022*

Citation:
Timmerman LR, Raghavan S and Borole AP (2022) Advancing Microbial Electrolysis Technology via Impedance Spectroscopy and Multi-Variate Analysis. Front. Energy Res. 10:756900. doi: 10.3389/fenrg.2022.756900

INTRODUCTION

Bioelectrochemical systems (BES) are an emerging technology that have shown tremendous promise employing biocatalysts attached to electrodes of electrochemical systems to generate energy or value added products from carbon sources in waste streams (Bajracharya et al., 2016). The two major classes of BES are Microbial Fuel Cells (MFC) which convert waste directly to electricity, and Microbial Electrolysis Cells (MEC) which harness the energy from an applied voltage to convert waste products into value added chemicals such as hydrogen. MEC technology has been proposed as an environmentally responsible and economic means of eliminating food waste–a significant contributor to greenhouse gas emissions–from landfills (Beegle and Borole, 2018; Huang et al., 2020; Satinover et al., 2020b). This application would also provide a "green" source of hydrogen which is a common chemical feedstock and a viable alternative to carbon based automotive fuels.

Remarkably efficient laboratory scale MEC for food and wastewater treatment have been demonstrated in the literature (Liang et al., 2011; Miller et al., 2019; Satinover et al., 2020a; Satinover et al., 2020b). Successful scale-up and commercialization of this promising technology will require accurate identification of the limiting processes in high performance systems and clever manipulation of design and operational parameters to meet large scale performance requirements (Borole et al., 2019; Leicester et al., 2020). One of the most powerful investigational tools available to aid MEC researchers in this quest is Electrochemical Impedance Spectroscopy (EIS) which has the capacity to deconvolute and quantify ohmic, kinetic, and mass transfer related impedances separately for the anodes and cathodes of electrolysis cells in concert with the application of an appropriate Equivalent Circuit Models (He and Mansfeld, 2009; Dominguez-Benetton et al., 2012; Agostino et al., 2017). These impedances can be considered energy losses, which provide information regarding the processes limiting cell performance.

Much of the existing BES EIS literature is devoted to the study of the more mature MFC technology and is often conducted in the whole cell (WC) or two electrode configuration preventing direct comparison of substrate oxidation at the bioanode, although there can be many similarities between the MFC and MEC systems (Miller et al., 2019). Thus, the existing MFC EIS literature can be used as a guide to MEC EIS studies so long as careful attention is paid to the experimental setup and reported results. For example, Ramasamy et al. investigated the impact of the initial biofilm growth on the kinetics and total internal impedance of a MFC *via* EIS in a manner that could be applied analogously to MECs (Ramasamy et al., 2008). The procedure they describe for determining the kinetic parameter exchange current (i_o) in an MFC can be used with minimal alteration to assess the kinetics of MEC anodes. Similarly, Agostino et al. report several EIS procedures in their MFC EIS study, which can be applied to MEC EIS studies (Agostino et al., 2017). This includes collecting and reporting EIS data for the system prior to the formation of any biofilm, which allows for accurate assignment of EIS related phenomena to physical processes. Lepage et al. conducted a multifactorial evaluation on the effects of temperature, phosphate buffer concentration, substrate concentration, and solution conductivity on MFC performance utilizing EIS to quantify the impedance response (Lepage et al., 2014). Their analysis allowed them to pinpoint exactly how and to what extent the shifts in operational parameters were impacting MFC performance. This type of analysis can easily be extended to characterize MEC systems.

Some MEC studies have begun to utilize EIS to optimize reactor design configurations and operating parameters. Borole et al. used EIS as a complementary technique to identify proton transport as a primary limitation to current production in high performance MEC and to quantify the impact of anode chamber flow rate and substrate concentration on whole cell impedance (Borole and Lewis, 2017). EIS has also been used as a criterion for judging the merit of design and operation decisions such as anode to cathode surface area ratios, optimal buffer concentration, electrode material selection, and electrode arrangement by selecting conditions or arrangements that minimize total impedance or balance anode and cathode impedance (Liang et al., 2011; Cai et al., 2016; Miller et al., 2019). Unfortunately, impedance parameters cannot be used as the sole criterion for judging the relative merit of selected design or operational conditions since choices that minimize impedance can result in unreasonable increases in material or operational costs (e.g., the optimal conditions identified by Miller, Singh et al. include a 110 mM Phosphate Buffer solution which would be uneconomical for most practical applications). Thus, systems designed for commercial operation will need to consider trade-offs between conditions that optimize performance and those that minimize cost. To assist researchers and entrepreneurs in the effort to make informed design decisions, studies must be conducted which consider both the impact and relative importance of operational and design parameters on system performance.

In this study, we began by monitoring the EIS spectra of a two-chamber MEC from abiotic conditions to a target current density of 10 A/m^2 to accurately assign portions of the spectra to the corresponding physical phenomena in service of developing an appropriate Equivalent Circuit Model (ECM). Once completed, an experimental Taguchi array was constructed and executed to simultaneously evaluate the impact of varying buffer concentration, applied cell potential, and anode flow rate on system performance *via* EIS. The resulting EIS spectra were then fit with the previously developed ECM to obtain individual impedance parameters related to ohmic, kinetic, and mass transfer processes. Summary statistics for each cell were also recorded for the runs. The resulting data were analyzed using multi-variate analysis to ascertain both the quantifiable impact and relative weight of buffer, applied potential, and flow rate on the response variables.

METHODS

MEC Construction

A two-chamber MEC was constructed with carbon felt as the anode material (0.64 cm thickness, CeraMaterials, Dingmans Ferry, PA) and a Ni-mesh as the cathode (100 mesh size, Anping County Longyi Mesh Manufacture Co., Ltd. China). A stainless-steel current collector was used in both the anode and the cathode. The anode was three dimensional (2.9 cm × 6.9 cm × 0.64 cm) to promote bacterial growth while the cathode was two dimensional (2.9 cm × 6.9 cm). The electrodes were separated by a 0.2 micron microporous membrane (Tisch Scientific). The electrodes were enclosed inside two acrylic end plates and rectangular pieces of a rubber gasket material with an inside volume of 14 ml for the anode and 7 ml for the cathode. Two identical duplicates were used in the experiment for replicate data generation referred to as reactor A and reactor B.

MEC Operation and Inoculation

A nutrient medium consisting of Wolfe's mineral and vitamin solution, plus 0.31 g/L NH_4Cl, 0.13 g/L KCl, and 50 mM phosphate buffer, adjusted to a pH of seven was sparged with

nitrogen to remove dissolved oxygen. This nutrient medium was initially free of sodium acetate and liquid food waste, described later. It was circulated from a 150 ml reservoir to the cell at a flow rate of 4 ml/min using a peristaltic pump for at least 1 day prior to inoculation to ensure the carbon felt anode was fully wetted and anaerobic. A flow rate of 4 ml/min of the previously described solution was maintained throughout the inoculation process. The cathode outlets were initially clamped but once the target current density was reached, the outlets were attached to vacuum sealed brine columns to measure hydrogen production (**Supplementary Figure S1**). The duplicate MECs constructed as detailed above were inoculated from existing duplicate MECs whose bioanodes had previously been enriched for electrogenic activity via the procedure outlined below. The previous generation of MEC's were operated in a configuration where the anode cell voltage was monitored and maintained below −0.2 V vs. Ag/AgCl by adjusting the cell voltage (WC configuration). The design of the parent electrolysis cells was nearly identical to that of the cells to be inoculated with the single exception being the thickness of the felt (1/4″ vs. 1/8″). The inoculation occurred by removing 1/4" diameter cores from the bottom middle of the enriched bioanodes with a coring tool and inserting them into holes of same size in the carbon felt of the newly constructed MECs. The inoculated reactors were initially operated in batch mode to prevent excessive substrate accumulation during the lag phase of microbial growth. The batches consisted of pure sodium acetate dissolved in DI water and introduced into the MEC at a concentration of 0.1 g/L. The MECs were poised in the WC configuration with the anode as the working electrode and the cathode as the counter and "effective" reference electrode, meaning the potential of the anode was set relative to the cathode (WC poising). The anode and cathode potentials were also continually monitored versus an Ag/AgCl reference electrode placed in the anode chamber. A Bio-Logic Potentiostat (Model VMP-3e, Knoxville, TN) was used to perform the experiments. The cell was initially held at a WC potential of 0.4 V until the anode voltage reached a potential of −0.4V vs. Ag/AgCl reference electrode (BASi, Inc., West Lafayette, IN), indicating secure biofilm attachment. Substrate was delivered continuously via an in-line syringe pump (Braintree Scientific, Inc., programmable syringe pump, Model BS-8000) at the anode inlet once the MEC reached a current output of 1 mA. Anode flow rate and media composition were held constant during the inoculation and growth period while cell potential and organic loading rate (OLR) were periodically adjusted in response to current output and anode potential until a target current density of 10 A/m^2 was reached. The continuously delivered substrate consisted of a mixture of sodium acetate and a 0.2 micron filtered, liquid food waste, the latter contributing 10% of the total chemical oxygen demand (COD). The food waste was generated from a food prep waste obtained from a local restaurant and contained vegetable and fruit discards. The liquid produced by squeezing the food prep waste was used in the MEC experiments, after filtration through a 0.2 micron filter. All other solutions were autoclaved prior to use to ensure aseptic conditions. Planktonic growth was monitored daily *via* a OD620 procedure, and fresh media was supplied as necessary to maintain a consistent environment for the bioanode.

TABLE 1 | Taguchi experimental array detailing the experimental conditions and order of trials.

#	Taguchi, p = 3, L = 3		
	Buffer	**Volt**	**Flow**
1	50	1.2	4
2	50	1.5	0.4
3	50	0.8	0.04
4	5	1.2	0.4
5	5	1.5	0.04
6	5	0.8	4
7	10	1.2	0.04
8	10	1.5	4
9	10	0.8	0.4

After reaching the target current density, the MEC were operated at nine different combinations of applied cell potential, buffer concentration, and anode flow rate detailed in **Table 1**. Applied potential was adjusted directly via EC-Lab software (Bio-Logic USA, Knoxville, TN) to reach the target values. The buffer concentration was varied *via* preparation of media solutions of differing buffer strengths while maintaining constant concentrations of the vitamins, minerals, and salts. The peristaltic pump used to maintain a flow rate of 4 ml/min was not capable of reaching the lower flow rates tested, so a syringe pump was used to deliver the media and the substrate directly to the MEC at the desired flow rates. Substrate concentration in the syringes was varied to maintain a constant OLR across trials. The syringes used to deliver the substrate and nutrient medium were autoclaved prior to use and primed with sparged substrate and nutrient medium solution. The pH of the media was adjusted to seven before each run. Three performance analysis experiments were executed after conducting preliminary analysis of the EIS data. These were carried out at constant applied potential with varying buffer concentration and anode flow rate. The buffer concentration was controlled in the manner described above. The flow rates were controlled *via* a peristaltic pump. Cathode gas was collected *via* inverted brine columns, while the anode headspace was sealed with a water trap.

Electrochemical Measurements

A chronoamperometry (CA) method predefined in EC-Lab software was used in concert with the Bio-Logic Potentiostat to poise the MEC at desired voltage levels and continuously collect current and voltage data during the inoculation and growth periods as well as in between EIS runs and during the performance analysis trials. The MECs were poised in the whole cell configuration with the anode acting as the working electrode and cathode acting as the counter electrode as well as the reference electrode. In the half cell EIS runs, the reference electrode lead was connected to the Ag/AgCl probe in the anode chamber to track the anode and cathode potentials. In the anode half-cell experiments, the anode served as the working electrode, and the cathode as the counter electrode, and vice versa for the cathode half-cell

experiments. All anode or cathode potentials reported in this study are vs. this Ag/AgCl reference electrode. For the performance analysis runs, COD analysis was coupled to the CA data to quantify COD removal and columbic efficiency (Lewis et al., 2015). Gas analysis conducted on a GC column (Agilent Technologies Inc, CP-Molsieve 5A, Part # CP7536) was used to quantify the composition of the cathode gas and anode headspace. This allowed for losses related to methanogenesis in the anodes of the MEC to be quantified. The CA method was also used to quantify a number of summary statistics for each of the run conditions including Anode Voltage, Open Circuit Voltage, Cathode Voltage, and Current. Cathode liquid samples were also taken during CA posing to quantify the pH levels in the cathode.

The EIS data was analyzed by fitting an equivalent circuit model (ECM) which generates pseudo-electrochemical parameters which can be broken down to represent anode and cathode impedances separately, as well as individually to assess the ohmic, kinetic, and mass transfer limitations of an MEC. Common configurations of ECM for MEC and MFC have included a resistor representing solution resistance connected in series to parallel combinations of resistors representing charge transfer reactions and constant phase elements representing the capacitive behavior of anodes or biofilms (Ramasamy et al., 2008; Liang et al., 2011; Yin et al., 2013; Agostino et al., 2017). Warburg elements are also included when mass transfer is expected to be a limiting factor in system performance. The key to any successful EIS ECM study is to ensure that the proposed ECM provides physically meaningful information about the system and satisfies goodness of fit criteria. To that end, the initial set of EIS measurements collected prior to inoculation and during the growth period at current outputs of 10, 15, and 20 mA (current density of 5, 7.5, and 10 A/m^2) were analyzed qualitatively to develop a physically meaningful and robust ECM. EIS measurements were taken in three electrode configurations with the anode and cathode serving as the working electrode for anode half-cell (AC) and cathode half-cell (CC) runs respectively with an Ag/AgCl reference electrode in the anode chamber. All EIS measurements in this study occurred over the frequency range of 100 kHz to 10 mHz to ensure the relevant physical phenomena were captured in the EIS spectrum. A 10 mV sinus amplitude was used for the perturbation of closed circuit runs to ensure a strong response signal, while a smaller 5 mV perturbation was used for open circuit (OCV) measurements to maintain low overpotential conditions. The EIS settings for the initial group of measurements included six points per decade in logarithmic spacing with the application of a built-in drift correction algorithm. The ECM developed from these initial runs was used to quantify the change in exchange current during the growth period via the Simplex method for multi-parameter fitting plus a randomize function to ensure unbiased starting parameters. Additional iterations were occasionally necessary to satisfy convergence criteria. The procedure for calculating exchange current from EIS data is laid out by Ramasamy et al. (2008). Briefly, exchange current can be calculated directly from charge transfer impedance *via* the relationship

$$R_{Ctr} = \frac{RT}{nFi_o} \quad (1)$$

where R is the universal gas constant in J/mol-K, T is the temperature in Kelvin, n is the number of electrons involved in the oxidation reaction per molecule of reactant (8 for acetate), F is Faraday's constant, and i_o is the exchange current in Amperes. The EIS measurements must be conducted at low overpotentials for **Eq 1** to be valid. Thus, exchange current calculations were derived from R_{ctr} values obtained at OCV EIS conditions. The OCV was determined by allowing the system to sit at open circuit until the anode voltage reading stabilized.

The EIS data for the Taguchi array was collected and analyzed in an analogous manner, but the following EIS settings were adjusted to improve the lower frequency data quality and boost acquisition speed. The drift correction was dropped for all frequencies and a multi-sine amplitude was used at frequencies below 1 Hz. Additionally, the number of data points per decade was increased to 10 as a means of enhancing the robustness of the EIS spectrum. The MECs were allowed to stabilize for a minimum of 5 h at each testing condition prior to any EIS measurements to ensure the system was at an equilibrium state. OCV data was also collected at each experimental condition and analyzed in the manner described previously to continue tracking the kinetic capacity of the system. All EIS data collected were fit with the previously developed ECM to quantify the impacts of the shifts in operational parameters on the total system impedance and individually the ohmic, kinetic, and mass transfer effects in the anode and cathode separately.

Multifactorial Experimental Matrix

Three operational parameters (buffer concentration, anode flow rate, and applied potential) were selected to be varied across three levels–a low, middle, and high condition. Buffer concentration was tested at 5, 10, and 50 mM. Applied voltages of 0.8, 1.2, and 1.5 V were investigated. Flow rates of 0.04, 0.4, and 4 ml/min were also studied. An orthogonal Taguchi (see **Table 1**) array was constructed based on varying three parameters at three levels. The resulting data was analyzed to evaluate the impact of the selected operational parameters on the system impedance evaluated *via* EIS, and the response of a group of summary statistics.

Multivariate Analysis

A set of experiments based on the Taguchi design, with buffer concentration, voltage and flow rate as factors was conducted. A large and diverse data set, consisting of EIS, Chronoamperometry, pH, and voltage measurements resulted from these experiments. The data was further leveraged to either infer or confirm the anticipated relationships, between the factors and the responses, statistically.

The main conclusions from the two types of analyses that were performed are presented below: First, the data was explored using the multivariate platform in JMP to check how the variables relate to each other. The analyses showed that many of the spectroscopic measurements were correlated hence it should be adequate to measure only a subset of the variables. This

preliminary investigation did not indicate a significant interaction between the factors on the responses. Second, based on the above analysis, a multivariate linear regression model, with buffer concentration, voltage and flow rate as factors was fitted to a selected set of noteworthy responses. The standard least square personality was used for fitting the model. The key results from this analysis are presented in **Table 3**.

RESULTS AND DISCUSSION

Model Development and Biofilm Growth

The Nyquist and Bode (Anode Cell) plots for the initial series of EIS runs (abiotic through 20 mA) are presented in **Figure 1**. Note that EIS data for the cathode cell was not collected for abiotic conditions as the addition of a microbial community to the anode was not expected to dramatically change the overall shape of the cathode spectrum. The AC Nyquist plot contains two distinct semicircles, both of which respond to the initial attachment of biofilm at the anode. The high frequency semicircle initially diminishes in diameter corresponding to diminishing impedance, but undergoes no additional shift with growth up to 20 mA. The low frequency semicircle undergoes a continuous shift from the abiotic condition through to 20 mA. These trends are mirrored on the Bode plots which show an initial shift in phase for the high frequency phenomena with minimal additional shifts up to 20 mA while the low frequency phenomenon undergoes a continuous phase shift through 20 mA. Based on this qualitative analysis, it was concluded that the high and low frequency phenomena corresponded to unique physical processes. The high frequency phenomena most likely corresponds to a redox process unrelated to the biocatalytic oxidation of acetate at the anode surface. This high frequency behavior in similar systems has been reported previously and has been attributed to the oxidation of soluble metal ions, the transfer of electrons at the anode/solution interface, and the effects of porous electrodes on EIS spectra (Ramasamy et al., 2009; Agostino et al., 2017; Rossi et al., 2020). Each of these conditions could reasonably be considered the case for the system studied but were not investigated further as the researchers were satisfied with the ability to distinguish between portions of the EIS spectra related to the bioelectrochemical oxidation of acetate and those related to other phenomena. The change with respect to time, or growth, of the lower frequency phenomena suggests that it most likely represents the oxidative activity of the electroactive biofilm. The CC Nyquist and Bode indicate that there may be two distinct phenomena occurring. Plots of the negative imaginary portion of impedance spectra vs. frequency can be used to determine the number of distinct constant phase elements which should be included into the ECM (Sevda et al., 2015). This analysis revealed that there only existed one relative maxima for each of the EIS spectra indicating that the high frequency phenomena most likely did not represent a distinct physical process. Additional analysis of the Nyquist and Bode plots demonstrated that after correcting for shifts in the high frequency intercept of the Nyquist plot which is known to represent solution + membrane conductivity, there was no significant response of the high frequency impedance during the growth period. Thus, it was determined that this portion of the spectrum was likely due to high frequency relaxation processes, similar to those reported by other groups previously (Dominguez-Benetton et al., 2012).

The preceding analysis was used to construct physically meaningful ECM depicted in **Figure 2** for both the anode and cathode of the duplicate MEC used in this study. As previously mentioned, a resistor is commonly used to represent solution + membrane resistance, which manifests as the high frequency real axis intercept of the Nyquist plot. This ECM element was used for both the anode and cathode models and was labeled R_1. The high frequency phenomena in both the anode and cathode were fit to a parallel combination of a constant phase element (CPE) and a resistor, labeled Q_2 and R_2 respectively. CPE consist of a coefficient Q and an α term to account for non-ideality. This non-ideality captured by the α term, which ranges from 0 to 1 depending on the deviation from ideal behavior, arises from the complexities of biological electron transfer that cannot be exactly captured by simple electrical circuit elements. The coefficient Q represents the magnitude of the pseudo capacitance. The resistor represents loss due to the transfer of charge in the system. In the anode, this combination of ECM elements represents the flow of charge from the carbon felt anode material to solution while the constant phase element represents the non-ideal capacitive behavior of the anode material. The connection to a physical process in the cathode is less clear, but it was modelled in this way as a means of separating potentially anomalous impedance data from the physically meaningful portion of the spectrum. The low frequency phenomena in the anode and cathode were modelled *via* a Randles cell, which includes a constant phase element connected in parallel to resistor and Warburg element connected to each other in series. The Randles cell is a common artifact of many EIS studies as it can account for capacitive, reaction, and mass transfer related impedances. In the case of the anode, the second constant phase element Q_3 represents the non-ideal capacitive behavior of the electroactive biofilm. The resistor R_3 accounts for the charge transfer resistance associated with the bioelectrochemical oxidation of acetate. The Warburg element selected, Wd_3 which consists of Rd_3 and td_3, utilized a convective diffusion model of mass transport to quantify the impedance related to the transport of substrate to the biofilm and the transport of protons away from the biofilm. For the cathode, the constant phase element represents the non-ideal capacitive behavior of the Ni-mesh electrode, while the resistor accounts for the charge transfer resistance related to the reduction of protons to form hydrogen. The Warburg element in this case accounts for the transport (convective diffusion) of protons to the surface of the electrode.

It should be noted that the numerical analysis in the section "Multivariate Analysis: Deviation from Mean" consists of data from reactor A only. Identical analysis was conducted for both duplicates, and the results presented herein for reactor A include only those that agree across duplicates. Similar analysis for reactor B can be found in the supplemental information (**Supplementary Table S1**). The EIS data from the inoculation and growth period was analyzed using the developed ECM at

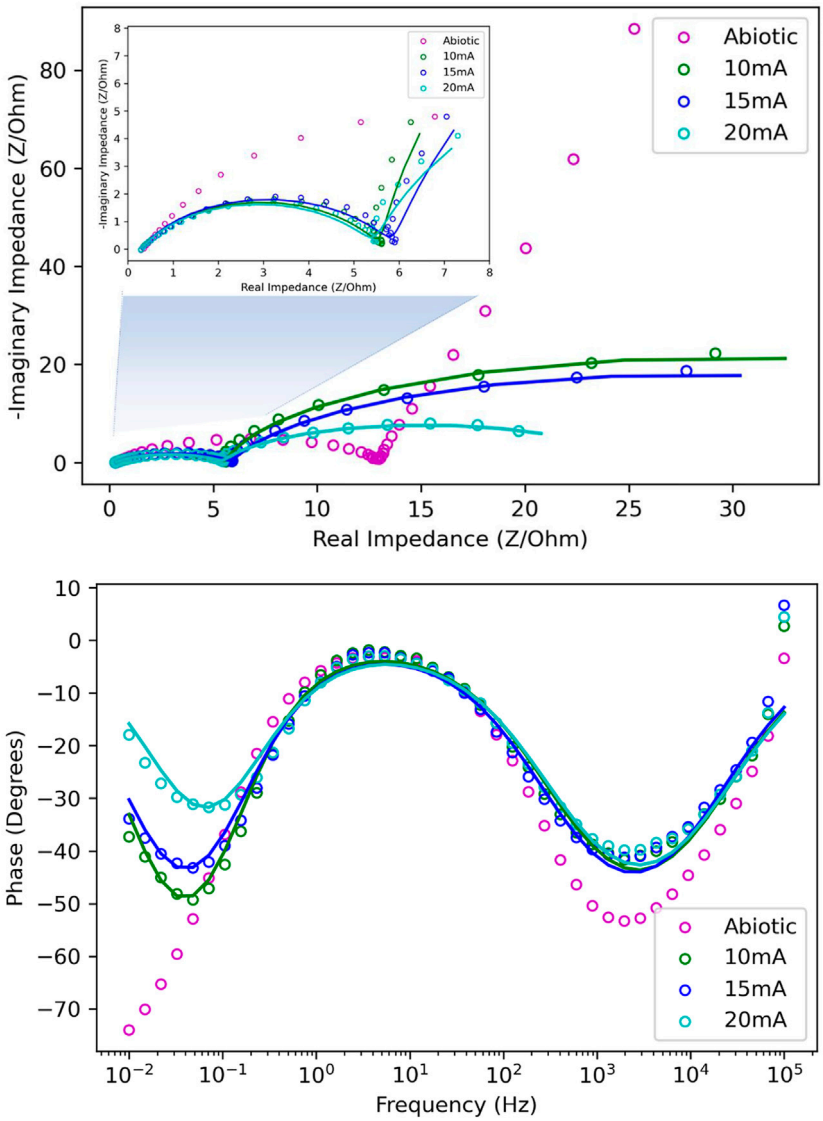

FIGURE 1 | Nyquist and Bode plots for inoculation and growth phases of MEC development. The ECM fit is included as a solid line overlaid on the raw data.

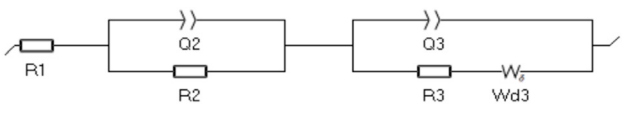

FIGURE 2 | ECM for both the anode and the cathode half cells.

OCV conditions to assess the change in kinetic capacity *via* quantification of the exchange current. The exchange current for bioelectrochemical oxidation of acetate was assumed to be zero for the abiotic condition since there was no biofilm or acetate present in the system. The exchange currents were calculated to be 3.34, 3.66, and 8.27 uA/cm^2 at the 10, 15, and 20 mA EIS runs respectively. These results indicate an order of magnitude improvement from those reported by Ramasamy et al. (2008). This marked improvement could be attributed to a number of factors, including improvements in cell design or due to the benefits of using inoculum that has been enriched for exoelectrogenesis used in the reactors studied in this investigation. The exchange current measured during this initial analysis was used as a baseline for assessing the kinetic performance of the system in later trials.

Multivariate Analysis: Deviation From Mean

The Taguchi array was executed according to the order listed in **Table 1** with EIS data collected for all trials and fit with the previously described ECM (**Supplementary Table S2**). Each EIS run resulted in 18 impedance parameters in accordance with the previously described ECM—9 for the anode and 9 for the cathode. **Table 2** provides the mean values for impedance

TABLE 2 | Mean values and percent deviation from overall average of relevant EIS parameters for the lowest, medium, and highest settings tested.

Buffer	Anode cell					
	Low	**Med**	**High**	**Mean**	**Low Med**	**Low High**
R_1	0.563	0.587	0.341	0.497	5%	−45%
Q_3	0.506	0.537	1.96	1.00	3%	146%
Rd_3	76.3	77.9	23.5	59.2	3%	−89%
Volt						
Rd_3	1.68	72.7	103	59.2	120%	172%
Flow						
Q_3	0.360	0.692	1.95	1.00	33%	159%
R_3	12.7	0.003	1.32	4.69	−272%	−244%
Rd_3	110.0	43.0	24.5	59.2	−113%	−145%
	Cathode Cell					
Buffer						
R_1	3.00	2.76	0.874	2.21	−11%	−96%
Q_3	0.006	0.010	0.014	0.010	35%	73%
R_3	16.9	17.3	8.26	14.1	3%	−61%
Flow						
Q_3	0.005	0.008	0.017	0.010	29%	117%
R_3	19.4	10.5	12.4	14.1	−62%	−49%
Rd_3	24.4	21.0	1.99	15.8	−22%	−142%

parameters at a given level for each independent variable. The table also includes the overall average for each impedance parameter, which is simply the average of all nine trials. The columns labeled Low Med and Low High compare the percent deviation of mean values for impedance parameters from the lowest value that a given independent variable was tested at to the middle and highest values. This deviation is normalized relative to the overall average for that impedance parameter. This form of analysis was adapted from a similar multifactorial study (Lepage et al., 2014). **Table 2** includes only those values which exhibited clear and reproducible trends across duplicates in response to the variation of the selected independent variables: buffer concentration, applied potential, and anode flow rate.

Effect of Buffer Concentration

The first entry lists the effect of buffer on R_1 which represents the solution and membrane resistance in the anode. This relationship can be considered a test for the validity of the analysis because the effect of buffer concentration on solution resistance is known *a priori*: since the buffer is prepared from a sodium-based salt, higher buffer concentrations should increase the conductivity of the electrolyte solution resulting in a decrease in solution resistance. The membrane resistance should remain unaffected. The data suggests that a 5% increase in solution resistance occurred as a result of increasing the buffer concentration from 5 to 10 mM. This 5% change is considered to be within experimental error. The cathode behaved similarly, showing little response to small increase in buffer concentration excluding the CPE. This difference in response could be due to differences in the electrode materials. The anode consists of carbon felt with a biofilm attached, whereas the cathode is a nickel mesh. In general, these findings are consistent with prior studies investigating similar buffer concentrations (Lepage et al., 2014). When the buffer concentration was increased to 50 mM, there was a more dramatic impact on the system's impedance response. R_1 decreased in both the anode and cathode as would be expected, although the effect was more pronounced in the cathode. The CPE in both the anode and cathode increased significantly while the mass transfer related impedance in the anode dropped off and the charge transfer resistance in the cathode diminished significantly. Increases in the magnitude of the CPE have previously been connected to improved system performance during growth phases (Martin et al., 2013; Lu et al., 2015), but it is interesting to note that operational parameters appear to have a similar impact. The decrease in mass transfer impedance in the anode is unsurprising as increased buffering capacity should aid in alleviating any proton related transport issues which have been shown to be limiting in previous studies (Borole and Lewis 2017). What is surprising is that there was no clear trend between buffer concentration and mass transfer impedance in the cathode. Rather, the only clear effect appears to be on charge transfer resistance which is typically associated with reaction kinetics.

Effect of Cell Voltage

The only clear trend associated with changes in applied potential was an increase in mass transfer related impedance in the anode. This trend aligns with the established relationship between applied potential and mass transfer related impedance in classical electrochemical systems: as applied potential increases, reaction kinetics become facile to the point that the reaction rate becomes dominated by mass transfer related impedance and further increases in applied potential do not result in increased current (Bard, 1980). This relationship does not translate directly to BES as these systems rely on biological mechanisms to produce electrons and generate current which often have preferred conditions (Lim et al., 2020). Nonetheless, this result suggests that at conditions conducive to rapid reaction rates and high current densities, mass transfer is an important consideration for system designs and operational parameter selection.

Effect of Anode Flow

Flow rate had a profound impact on the impedance response of both the anode and the cathode. In general, increased anode flow rate resulted in a larger magnitude of CPE and lower charge transfer and mass transfer related impedances which indicates that increasing flow rate had a significant positive effect on system performance. The charge transfer resistance initially decreased when the flow rate was adjusted from the 0.04 to 0.4 ml/min, but then increased slightly when the flow rate was further increased to 4 ml/min. This slight increase in charge transfer resistance at the highest condition is most likely indicative of a plateau as opposed to deleterious impacts from the high flow condition (Aaron et al., 2010). The increase in the CPE coefficient is unsurprising and in accordance with the previous discussion regarding CPE. Of interest is the impact of flow on the mass transfer impedance in both the cathode and the anode. The flow rate manipulated directly in this study was the flow of media through the anode

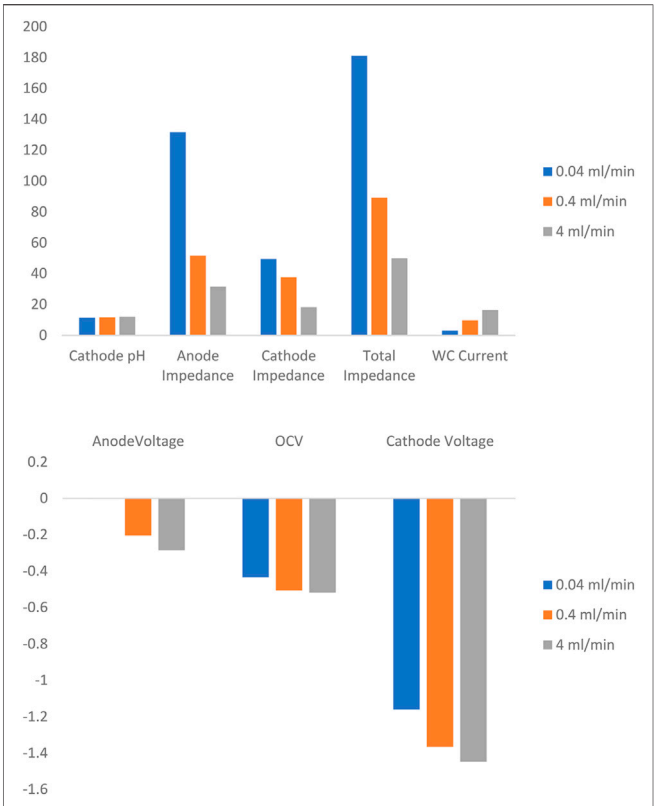

FIGURE 3 | Average response of selected summary statistics to increasing flow rates ranging from 0.04 ml/min to 4 ml/min. The voltage measurements are all in Volts, Impedance measurements are in Ohms, and Current measurements are in Milliamperes.

chamber, which was separated from the cathode chamber by a microporous membrane. It is possible that the increased flow rate through the anode resulted in a greater flux of ions across the membrane thereby enhancing the transport rate of protons to the cathode surface. Flow rate and recirculation of liquid, both have been shown to have a significant effect on the performance of MEC, and the high flow condition was the only one for which the media + substrate was recirculated (Lewis and Borole, 2016). However, recirculation may not have played a significant role on the system studied here as the substrate was primarily acetate, which can be oxidized by electrogens directly without the need for generation and processing of intermediates. This relationship between anode flow rate and cathode mass transfer impedance is especially perplexing due to the nature of how anode and cathode overpotentials interact in a MEC poised in the whole cell configuration. Any process condition that facilitates the oxidation of acetate by the biofilm will reduce the overpotential necessary to achieve a given rate of current production (Ki et al., 2016). MEC poised under whole cell conditions will experience simultaneous decreases in the anode and cathode potentials. However, the decrease in cathode potential translates to an increase in overpotential at the cathode since a reduction reaction is occurring there. This more negative overpotential should result in an enhanced depletion rate of protons at the cathode surface resulting in extended concentration gradients and additional mass transfer impedance.

TABLE 3 | Strength of correlation (based on *p* values) and the R^2 values for correlations between investigational parameters and response variables.

Response	Factor correlation			Fit (R^2)
	Buffer	Voltage	Flow	
R_1 Anode	Strong	None	None	0.89
R_1 Cathode	Strong	None	None	0.83
Q_3 Cathode	None	None	Strong	0.4
a_3 Cathode	None	Strong	Strong	0.69
R_3 Cathode	Strong	None	None	0.39
Rd_3 Anode	Weak	Strong	Weak	0.79
Rd_3 Cathode	None	None	Strong	0.25
Summary data				
Anode Voltage	None	Strong	Strong	0.75
OCV	None	None	Strong	
Cathode Voltage	None	Weak	Strong	0.45
Cathode Impedance	Strong	None	Strong	0.47
Total Impedance	Weak	Weak	Strong	0.77
I_o	Strong	None	None	0.47
I	Strong	None	Strong	0.69

Statistical Analysis of the Results

Additional mean value analysis was conducted on a series of summary statistics, which were chosen to represent the overall performance of the system at a given condition. **Figure 3** illustrates the variation of these selected summary statistics with respect to flow rate. The *x*-axis delineates which parameter the observations apply to, and the *y*-axis units vary accordingly for each measurement. Clear trends for each of the statistics is clearly presented in the chart. Anode, OCV, and Cathode potential all decrease with increasing flow which implies that flow rate has a salubrious effect on the overpotentials required at the anode (working electrode). Anode, cathode, and correspondingly total cell impedance are also clearly beneficiaries of the effects of increased flow rate. Lastly, current production in the MEC is also strongly positively correlated to flow rate. This analysis suggests that flow is a dominant factor in determining overall system performance.

Multivariate Analysis: Correlations

More statistically rigorous analysis was conducted using the JMP software package to test for and evaluate correlations between buffer concentration, applied potential, and flow rate and the previously discussed response variables. The response variables which were found to be strongly correlated to at least one of the independent variables are included in **Table 3**. The statistical significance of the correlations was evaluated using a t test. A *p* value of 0.05 was set as the cut off for considering a response variable as a strong function of one or more of the independent variables. Additional consideration was given to factors that failed the *p* test for significance but had a dramatic impact on the R^2 value for the linear correlation fit. Plots of the experimental values vs. predicted values and 95% confidence

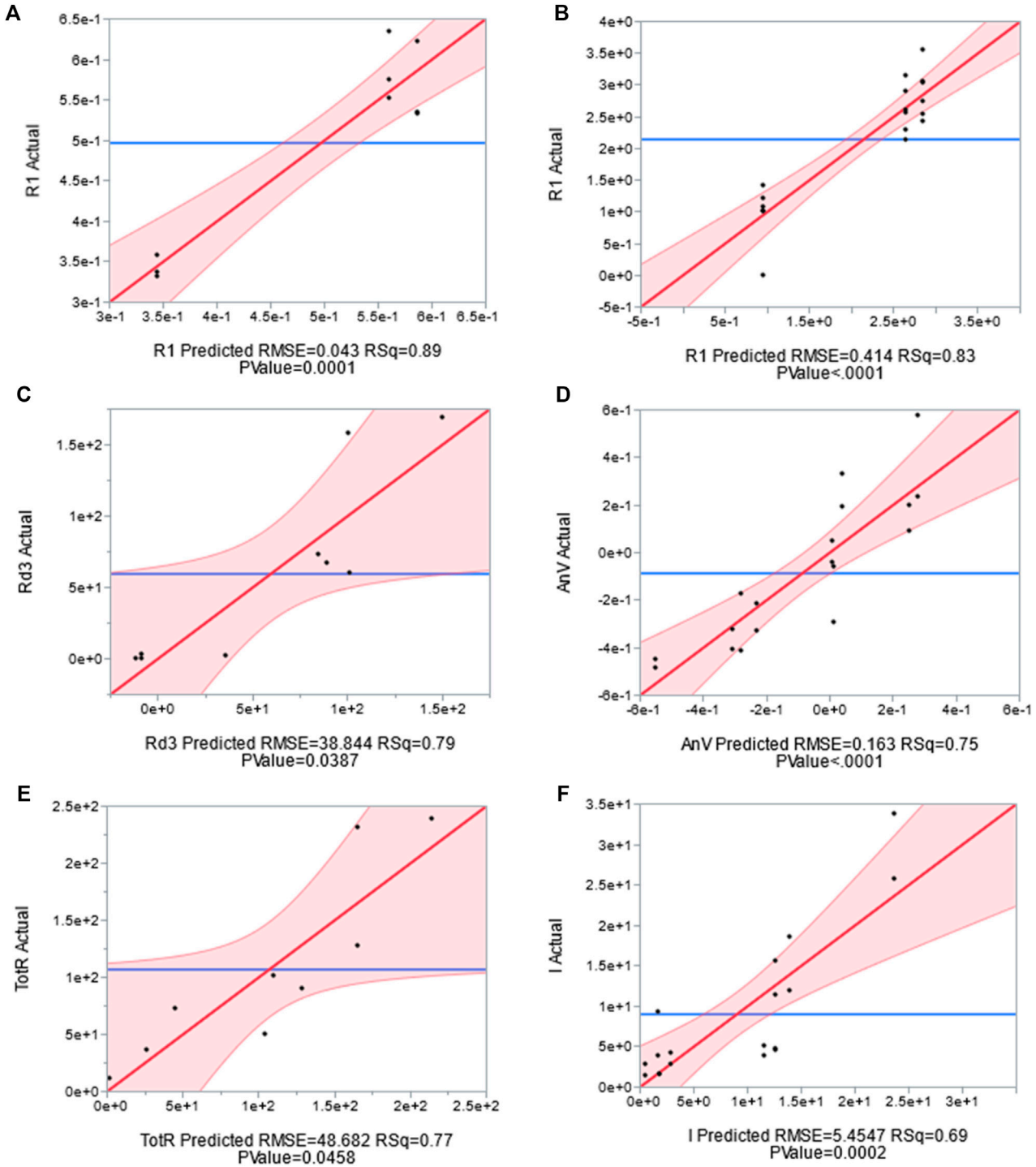

FIGURE 4 | Actual vs. Predicted plot for correlations generated via multivariate analysis for **(A)** R_1 Anode, **(B)** R_1 Cathode, **(C)** Rd_3 Anode, **(D)** AnV: Anode Voltage, **(E)** TotR: Total Impedance, and **(F)** IActual: Whole Cell Current. The experimentally determined values for the response variables are plotted on the *y* axis while the predicted responses as a function of buffer, flow rate, and applied potential are plotted on the *x* axis. The shaded region represents 95% confidence interval, and the quality of prediction can be assessed by evaluating the distance of each point from the solid red line. RMSE: Room mean squared error, RSq: square of the correlation coefficient.

intervals for correlations between the three independent variables and response factors are presented for physically interesting correlations in **Figure 4** with 95% confidence intervals. These plots provide a strong sense of how well the behavior of the given response can be predicted by flow rate, buffer concentration, and applied voltage.

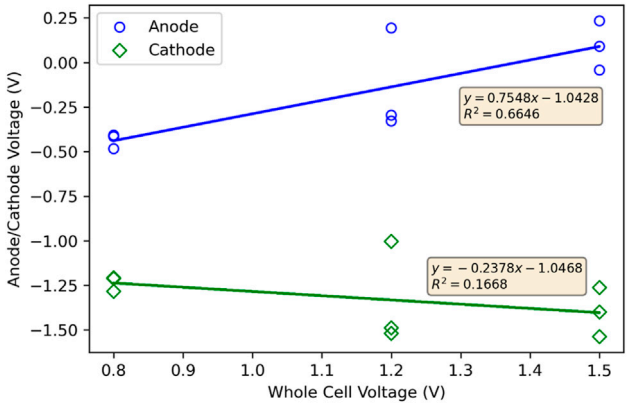

FIGURE 5 | Influence of cell voltage on anode (blue circles) vs. cathode (green diamonds) half-cell voltages. The majority of the shift occurs in the anode voltage indicating the need to operate the cell voltage under 1.5V.

The data from **Table 3** is in relatively good agreement with the analysis presented in the previous section, but it provides additional details regarding the relative weight of each independent variable on the response factors. First off, R_1 in both the anode and cathode is confirmed to be a strong function of buffer concentration as predicted by basic physics and the analysis of the preceding section. The R^2 values indicate that for the given data set, variations in buffer concentration account for upwards of 80% of the variation in the measured R_1. Charge transfer resistance in the cathode is also a strong function of buffer concentration, but the mass transfer impedance parameters in both the anode and the cathode are shown to be weak functions of buffer concentration. This is surprising since increased buffer concentration would be expected to facilitate the transport of protons out of the anode to the cathode. The data also reveals a strong connection between buffer concentration and anode exchange current, a kinetic parameter. This suggests that the phosphate buffer may have a greater impact on the kinetics of the system rather than the mass transfer by providing local buffering capacity at the biofilm surface to help maintain biologically ideal pH as opposed to improving the longer distance transport of protons from anode to cathode.

Voltage was shown to strongly influence both the mass transfer impedance in the anode and the anode voltage (in concert with flow rate). The data suggests that voltage is the primary factor influencing the mass transfer impedance in the anode, and that a correlation developed including the impacts of buffer concentration and flow rate can account for upwards of 79% of the variation of Rd_3 in the anode for the given data set. This comes as no surprise given the discussion of the previous section. An additional interaction of interest is the impact of applied potential on the anode voltage. The anode voltage can be used as an indicator of how efficiently the anode is operating. The lower the overpotential at which the anode can be operated and still produce a high current density, the more efficiently the system will operate since less energy is devoted to shifting the potential of the electrode away from its equilibrium state. Understanding the relationship between applied potential and anode voltage is key to selecting appropriate poising conditions. It may seem obvious to state that applied potential is correlated to anode voltage, but the distribution of increases or decreases in applied potential across the anode and cathode are not intuitive. Cathode voltage was found to be only weakly correlated to applied potential pointing to an uneven distribution of shifts in applied potential across the cell. The distribution is approximately 76% in anode and 24% in cathode (**Figure 5**). At higher cell potentials, the anode voltage becomes positive which may not be ideal for the exoelectrogens to grow or to generate current during production phase of MEC operation.

The results also provide a more detailed look at the influence of flow on the performance of the system. The CPE and mass transfer related impedance in the cathode are both shown to be strong functions of flow, while mass transfer related impedance in the anode is only a weak function of anode flow rate. This is another surprising result as it suggests that flow rate disproportionately relieves mass transfer issues in the cathode cell even though the direct effect of increased flow rate should be realized in the anode. This may be because the proton gradients in the cathode between the membrane and the electrode are steep. A boundary layer effect may be occurring as flow rate increases on the anode side affecting the submicron liquid layer on the cathode side due to the flow in the anode across the membrane. Lastly, the multivariate analysis emphatically confirms that flow rate through the system is the dominating factor governing most of the summary level performance statistics. All of the summary statistics, with the exception of exchange current, are strong functions of flow rate. Since exchange current is a kinetic parameter which should remain uninfluenced by mass transfer related phenomena, and all of the other parameters are in at least some way influenced by mass transfer, it is probable that flow rate was the dominating factor controlling mass transfer in the system.

Correlation Extension and Performance Analysis

It was concluded based on the deviation from mean analysis that flow rate and buffer concentration had the most pronounced effects on the performance of the system. It was also evident from the current production data and previous experimental observations that 1.2 V was the optimal setting for maximum current production. Thus, three performance analysis experiments were conducted at a constant voltage of 1.2 V while the buffer concentration and flow rate were varied over three trials in order to study the effects of buffer concentration and flow rate on performance in a high current producing system. The buffer concentrations and flow rate pairings were (10 mM, 4 ml/min), (10 mM, 10 ml/min), and (50 mM, 4 ml/min).

The correlations developed *via* multivariate analysis of the Taguchi experimental series were used to predict the performance of the MEC at 10 ml/min flow rate 10 mM buffer concentration and determine the extent to which they could provide useful predictions of performance outside of the tested ranges. The physically relevant correlations with R^2 values of at least 0.60 were considered. The results reveal that the only parameter accurately predicted by the correlations was solution resistance. This is not a

particularly interesting prediction since solution resistance was shown to be a function of buffer concentration only and the condition tested (10 mM) was a part of the Taguchi experimental set. The correlation overpredicted the impact of 10 ml/min flow on all of the other performance-based parameters including current, anode voltage, and the two impedance parameters. This suggests that there is likely a plateau in the relative improvements that additional increases in flow rate above 4–10 ml/min would have on the system's performance. Similar plateau behavior has been demonstrated in prior MFC studies (Aaron et al., 2010). The predictive capacity of the linear multivariate model could be improved by increasing the experimental range and investigating quadratic and interaction effects.

CONCLUSION

The impact of voltage, buffer concentration, and flow rate on MEC impedance and performance were studied according to a Taguchi experimental array. Additional performance analysis was carried out at selected conditions as an orthogonal method of validating the information obtained *via* ECM of EIS spectra. All three parameters were observed to have some degree of impact on the system, although the impedance parameters affected, and the magnitude of impact was inconsistent. Voltage was only weakly correlated to changes in performance as there was a trade off from increases in voltage between improving the kinetics in the system and introducing mass transfer impedances. Buffer concentration had a dramatic impact on the solution resistance as expected and a moderate impact on the observed charge transfer resistance. This result was somewhat surprising as the expectation was that buffer concentration would be correlated with mass transfer impedances due to impacts on the proton transport mechanisms in MEC. Flow was shown to be a dominating factor controlling system performance in MEC. Increasing the flow rate from 0.04 to 4 ml/min resulted in significant improvements to the mass transfer in the system, specifically in the cathode. This result shows that for the systems studied in this investigation, flow rate disproportionately affects the cathode performance. The EIS observations were corroborated with data from separate performance analysis runs, which showed flow rate had a distinct positive impact on cathode efficiency, but a negative effect on columbic efficiency in the anode. The failure of the correlations developed in this work to adequately explain the impact of flow outside of the range of values tested indicates that the linear multivariate model needs to be augmented by adding quadratic and interaction effects and by expanding the range of experimental data. Experimental constructs, including those based on Response Surface Design can be applied towards this end. Overall, the results of this study indicate that EIS can be an effective tool for identifying and quantifying factors limiting system performance in the anode and cathode separately and for subsequent determination of optimum operating conditions.

DATA AVAILABILITY STATEMENT

The original contributions presented in the study are included in the article/**Supplementary Material**, further inquiries can be directed to the corresponding author.

AUTHOR CONTRIBUTIONS

AB created an outline of the manuscript and coordinated content with the co-authors. LT conducted most of the experiments and initial data analysis. AB supported the construction of the MECs and experimental set up. SR did all the statistical analysis and helped write the section on multi-variate analysis. LT wrote the first draft of the manuscript and AB and SR contributed to the editing process to refine the contents into final version.

FUNDING

LT was partially supported by the LaunchTN program from the state of Tennessee. The LaunchTN Summer Internship Program provides talented college students with a paid opportunity to work with a growing startup or ecosystem builder in Tennessee. The 200+ alumni consistently share their diverse experiences and relationships developed in the summer program are memorable, enjoyable, and highly relevant to anyone pursuing an entrepreneurial path.

SUPPLEMENTARY MATERIAL

The Supplementary Material for this article can be found online at: https://www.frontiersin.org/articles/10.3389/fenrg.2022.756900/full#supplementary-material

REFERENCES

Aaron, D., Tsouris, C., Hamilton, C. Y., and Borole, A. P. (2010). Assessment of the Effects of Flow Rate and Ionic Strength on the Performance of an Air-Cathode Microbial Fuel Cell Using Electrochemical Impedance Spectroscopy. *Energies* 3 (4), 592–606. doi:10.3390/en3040592

Agostino, V., Ahmed, D., Sacco, A., Margaria, V., Armato, C., and Quaglio, M. (2017). Electrochemical Analysis of Microbial Fuel Cells Based on Enriched Biofilm Communities from Freshwater Sediment. *Electrochim. Acta* 237, 133–143. doi:10.1016/j.electacta.2017.03.186

Bajracharya, S., Sharma, M., Mohanakrishna, G., Dominguez Benneton, X., Strik, D. P. B. T. B., Sarma, P. M., et al. (2016). An Overview on Emerging Bioelectrochemical Systems (BESs): Technology for Sustainable Electricity, Waste Remediation, Resource Recovery, Chemical Production and beyond. *Renew. Energ.* 98, 153–170. doi:10.1016/j.renene.2016.03.002

Bard, A. J. (1980). *Electrochemical Methods : Fundamentals and Applications*. New York: Wiley.

Beegle, J. R., and Borole, A. P. (2018). Energy Production from Waste: Evaluation of Anaerobic Digestion and Bioelectrochemical Systems Based on Energy Efficiency and Economic Factors. *Renew. Sustain. Energ. Rev.* 96, 343–351. doi:10.1016/j.rser.2018.07.057

Borole, A. P., and Lewis, A. J. (2017). Proton Transfer in Microbial Electrolysis Cells. *Sustain. Energ. Fuels* 1 (4), 725–736. doi:10.1039/c7se00034k

Borole, A. P., Tiquia-Arashiro, S. M., and Pant, D. (2019). "Understanding Bioelectrochemical Limitations via Impedance Spectroscopy. Microbial Electrochemical Technologies," in *Microbial Electrochemical Technologies* (Boca Raton: CRC Press), 39–56.

Cai, W., Liu, W., Han, J., and Wang, A. (2016). Enhanced Hydrogen Production in Microbial Electrolysis Cell with 3D Self-Assembly Nickel Foam-Graphene Cathode. *Biosens. Bioelectron.* 80, 118–122. doi:10.1016/j.bios.2016.01.008

Dominguez-Benetton, X., Sevda, S., Vanbroekhoven, K., and Pant, D. (2012). The Accurate Use of Impedance Analysis for the Study of Microbial Electrochemical Systems. *Chem. Soc. Rev.* 41 (21), 7228–7246. doi:10.1039/c2cs35026b

He, Z., and Mansfeld, F. (2009). Exploring the Use of Electrochemical Impedance Spectroscopy (EIS) in Microbial Fuel Cell Studies. *Energy Environ. Sci.* 2 (2), 215–219. doi:10.1039/b814914c

Huang, J., Feng, H., Huang, L., Ying, X., Shen, D., Chen, T., et al. (2020). Continuous Hydrogen Production from Food Waste by Anaerobic Digestion (AD) Coupled Single-Chamber Microbial Electrolysis Cell (MEC) under Negative Pressure. *Waste Manage.* 103, 61–66. doi:10.1016/j.wasman.2019.12.015

Ki, D., Popat, S. C., and Torres, C. I. (2016). Reduced Overpotentials in Microbial Electrolysis Cells through Improved Design, Operation, and Electrochemical Characterization. *Chem. Eng. J.* 287, 181–188. doi:10.1016/j.cej.2015.11.022

Leicester, D. D., Amezaga, J. M., Moore, A., and Heidrich, E. S. (2020). Optimising the Hydraulic Retention Time in a Pilot-Scale Microbial Electrolysis Cell to Achieve High Volumetric Treatment Rates Using Concentrated Domestic Wastewater. *Molecules* 25 (12), 2945. doi:10.3390/molecules25122945

Lepage, G., Perrier, G., Merlin, G., Aryal, N., and Dominguez-Benetton, X. (2014). Multifactorial Evaluation of the Electrochemical Response of a Microbial Fuel Cell. *RSC Adv.* 4 (45), 23815–23825. doi:10.1039/c4ra03879g

Lewis, A. J., and Borole, A. P. (2016). Understanding the Impact of Flow Rate and Recycle on the Conversion of a Complex Biorefinery Stream Using a Flow-Through Microbial Electrolysis Cell. *Biochem. Eng. J.* 116, 95–104. doi:10.1016/j.bej.2016.06.008

Lewis, A. J., Ren, S., Ye, X., Kim, P., Labbe, N., and Borole, A. P. (2015). Hydrogen Production from Switchgrass via an Integrated Pyrolysis-Microbial Electrolysis Process. *Bioresour. Technol.* 195, 231–241. doi:10.1016/j.biortech.2015.06.085

Liang, D.-W., Peng, S.-K., Lu, S.-F., Liu, Y.-Y., Lan, F., and Xiang, Y. (2011). Enhancement of Hydrogen Production in a Single Chamber Microbial Electrolysis Cell through Anode Arrangement Optimization. *Bioresour. Techn.* 102 (23), 10881–10885. doi:10.1016/j.biortech.2011.09.028

Lim, S. S., Fontmorin, J.-M., Izadi, P., Wan Daud, W. R., Scott, K., and Yu, E. H. (2020). Impact of Applied Cell Voltage on the Performance of a Microbial Electrolysis Cell Fully Catalysed by Microorganisms. *Int. J. Hydrogen Energ.* 45 (4), 2557–2568. doi:10.1016/j.ijhydene.2019.11.142

Lu, Z., Girguis, P., Liang, P., Shi, H., Huang, G., Cai, L., et al. (2015). Biological Capacitance Studies of Anodes in Microbial Fuel Cells Using Electrochemical Impedance Spectroscopy. *Bioproc. Biosyst. Eng.* 38 (7), 1325–1333. doi:10.1007/s00449-015-1373-z

Martin, E., Savadogo, O., Guiot, S. R., and Tartakovsky, B. (2013). Electrochemical Characterization of Anodic Biofilm Development in a Microbial Fuel Cell. *J. Appl. Electrochem.* 43 (5), 533–540. doi:10.1007/s10800-013-0537-2

Miller, A., Singh, L., Wang, L., and Liu, H. (2019). Linking Internal Resistance with Design and Operation Decisions in Microbial Electrolysis Cells. *Environ. Int.* 126 (C), 611–618. doi:10.1016/j.envint.2019.02.056

Ramasamy, R. P., Ren, Z., Mench, M. M., and Regan, J. M. (2008). Impact of Initial Biofilm Growth on the Anode Impedance of Microbial Fuel Cells. *Biotechnol. Bioeng.* 101 (1), 101–108. doi:10.1002/bit.21878

Ramasamy, R. P., Gadhamshetty, V., Nadeau, L. J., and Johnson, G. R. (2009). Impedance Spectroscopy as a Tool for Non-intrusive Detection of Extracellular Mediators in Microbial Fuel Cells. *Biotechnol. Bioeng.* 104 (5), 882–891. doi:10.1002/bit.22469

Rossi, R., Hall, D. M., Wang, X., Regan, J. M., and Logan, B. E. (2020). Quantifying the Factors Limiting Performance and Rates in Microbial Fuel Cells Using the Electrode Potential Slope Analysis Combined with Electrical Impedance Spectroscopy. *Electrochim. Acta* 348, 136330. doi:10.1016/j.electacta.2020.136330

Satinover, S. J., Rodriguez, M., Campa, M. F., Hazen, T. C., and Borole, A. P. (2020a). Performance and Community Structure Dynamics of Microbial Electrolysis Cells Operated on Multiple Complex Feedstocks. *Biotechnol. Biofuels* 13 (1), 169. doi:10.1186/s13068-020-01803-y

Satinover, S. J., Schell, D., and Borole, A. P. (2020b). Achieving High Hydrogen Productivities of 20 L/L-day via Microbial Electrolysis of Corn stover Fermentation Products. *Appl. Energ.* 259, 114126. doi:10.1016/j.apenergy.2019.114126

Sevda, S., Chayambuka, K., Sreekrishnan, T. R., Pant, D., and Dominguez-Benetton, X. (2015). A Comprehensive Impedance Journey to Continuous Microbial Fuel Cells. *Bioelectrochemistry* 106 (Pt A), 159–166. doi:10.1016/j.bioelechem.2015.04.008

Yin, Y., Huang, G., Tong, Y., Liu, Y., and Zhang, L. (2013). Electricity Production and Electrochemical Impedance Modeling of Microbial Fuel Cells under Static Magnetic Field. *J. Power Sourc.* 237, 58–63. doi:10.1016/j.jpowsour.2013.02.080

Conflict of Interest: Authors LT and AB were employees of Electro-Active Technologies at the time the study was conducted.

The remaining author declares that the research was conducted in the absence of any commercial or financial relationships that could be construed as a potential conflict of interest.

Publisher's Note: All claims expressed in this article are solely those of the authors and do not necessarily represent those of their affiliated organizations, or those of the publisher, the editors and the reviewers. Any product that may be evaluated in this article, or claim that may be made by its manufacturer, is not guaranteed or endorsed by the publisher.